

**Insight into the evolution of nidovirus endoribonuclease based on the finding that
Nsp15 from porcine deltacoronavirus functions as a dimer**

Anjun Zheng^{1,2*}, Yuejun Shi^{1,2,3*}, Zhou Shen^{1,2}, Gang Wang^{1,2}, Jiale Shi^{1,2}, Qiqi Xiong³, Liurong Fang^{1,2}, Shaobo Xiao^{1,2}, Zhen F. Fu⁴, Guiqing Peng^{1,2#}

From the ¹State Key Laboratory of Agricultural Microbiology, College of Veterinary Medicine, Huazhong Agricultural University; ²Key Laboratory of Preventive Veterinary Medicine in Hubei Province, The Cooperative Innovation Center for Sustainable Pig Production; ³College of Life Science and Technology, Huazhong Agricultural University; ⁴Departments of Pathology, College of Veterinary Medicine, University of Georgia, Athens, GA 30602, USA.

Running Title: *The evolution of nidovirus endoribonuclease*

* These authors contributed equally to this work.

To whom correspondence should be addressed: Guiqing Peng: State Key Laboratory of Agricultural Microbiology, College of Veterinary Medicine, Huazhong Agricultural University, 1 Shi-zi-shan Street, Wuhan, 430070, China;

pengggq@mail.hzau.edu.cn; Tel. +86 18071438015; Fax. +86 27 87280480.

Keywords: Nidovirus, endoribonuclease, oligomerization, PDCoV Nsp15, evolution

Abstract

Nidovirus endoribonucleases (NendoUs) include Nsp15 from coronaviruses and Nsp11 from arteriviruses, both of which have been reported to participate in the viral replication process and in the evasion of the host immune system. Results from a previous study of coronaviruses SARS-CoV, HCoV-229E and MHV Nsp15 indicate that it mainly forms a functional hexamer, whereas Nsp11 from the arterivirus PRRSV is a dimer. Here, we found that porcine deltacoronavirus (PDCoV) Nsp15 primarily exists as dimers and monomers *in vitro*. Biological experiments reveal that a PDCoV Nsp15 mutant lacking the first 27 amino acids of the N-terminal domain (NTD, Asn-1 - Asn-27) forms more monomers and displays decreased enzymatic activity, indicating that this region is important for its dimerization. Moreover, multiple sequence alignments and three-dimensional structural analysis indicated that the C-terminal region (His-251 - Val-261) of PDCoV Nsp15 is 10 amino acids shorter and forms a shorter loop than that formed by

the equivalent sequence (Gln-259 - Phe-279) of SARS-CoV Nsp15. This result may explain why PDCoV Nsp15 failed to form hexamers. We speculate that NendoUs may have originated from XendoU endoribonucleases (XendoUs) forming monomers in eukaryotic cells and that NendoU from arterivirus gained ability to form dimers and that the coronavirus variants then evolved the capacity to assemble into hexamers. We further propose that PDCoV Nsp15 may be an intermediate in this evolutionary process. Our findings provide a theoretical basis for improving our understanding of NendoU evolution and offer useful clues for designing drugs and vaccines against nidoviruses.

Nidoviruses are positive-sense, single-stranded, enveloped RNA viruses with genome sizes ranging from approximately 12.7 to 31.7 kb; these viruses include the families of *Coronaviridae*, *Arteriviridae*, *Roniviridae*, and *Mesoniviridae* (1-3). Nidoviruses are found

in a broad range of hosts. Coronaviruses and arteriviruses mainly infect mammals, causing digestive, respiratory, neurological and immune-mediated diseases, which result in enormous economic losses and threatening public health (4-8). Coronaviruses are currently classified into 4 genera; these are *Alphacoronavirus*, *Betacoronavirus*, *Gammacoronavirus*, and *Deltacoronavirus*. Among coronaviruses, *Deltacoronavirus* has the smallest genome, ranging in size from approximately 25.4 to 26.6 kb (4). In contrast to coronaviruses, arteriviruses possess the smallest genomes of all nidoviruses; their genomes are approximately 12.7 to 15.7 kb in size (9, 10).

Nidoviruses contain 5' and 3' untranslated regions (UTRs) at the terminal regions of their genomes, and they utilize a discontinuous negative-stranded RNA synthesis model to generate subgenomic (sg) mRNA (11, 12). They have similar genomic organizations in which the two largest overlapping open reading frames (ORF1a and ORF1b) are located within the 5' proximal two-thirds of the genome and a ribosome frame-shifting event is involved in the translation process (13, 14). The viral RNA can be translated into 12 or 13 nonstructural proteins (nsps) in arteriviruses and 16 nsps in most coronaviruses to exert different biological functions, such as the formation of double-membrane vesicles (DMVs) and replication-transcription complexes (RTCs) formation (3, 15, 16). Viral RNA synthesis has been observed in DMVs of SARS-CoV and MHV (15, 17). Among the nsps found in *Nidovirales*, NendoU is unique and can both excise single and double-stranded RNAs and specifically recognize uridylylates to produce 2'-3'-cyclic phosphodiester products (5, 18). The DMVs are associated with the

production of double-stranded RNA intermediates and can sequester them away from host dsRNA sensors to prevent the activation of the host innate immune response (15). A recent study reported that the coronavirus Nsp15 cooperates with the viral replication complex to limit the exposure of viral dsRNA to host dsRNA sensors, thereby enabling the evasion of the host cell immune system (15, 19). In addition, the inhibition of IFN- β induction has been verified in PRRSV nsp11, but further investigations need to be conducted because a cytotoxic effect of wild-type nsp11 resulting in IFN- β inhibition was not excluded (20, 21). Regardless of whether Nsp11 contributes to the decline in innate immune functions, its importance in viral replication has been established (22).

Among the *Coronaviridae*, SARS-CoV Nsp15 was first shown to have NendoU activity *in vitro* (23); similar findings were then obtained for MHV, HCoV-229E, turkey coronavirus (24-27), and PRRSV (5). However, not all nidoviruses possess NendoU activity; some examples are the insect nidovirus Nam Dinh virus and roniviruses, all of which lack the EndoU domain (1, 28). The active sites of three catalytic residues (two histidines and one lysine) in NendoU are highly conserved in its counterpart, XendoU (19, 24), an endoribonuclease found in eukaryotes that processes the intron-encoded box C/D U16 small nucleolar RNA from its host pre-mRNA and produces 2'-3'-cyclic phosphate termini (29). An intriguing finding regarding NendoU and XendoU is the difference in their requirement for the manganese ion. XendoU is a monomer and requires Mn^{2+} (29, 30). Except for turkey coronavirus Nsp15, Mn^{2+} is generally essential for the catalytic activity of coronavirus Nsp15 (25, 31). However, Mn^{2+}

is dispensable and, to some extent, even inhibits the activity of PRRSV Nsp11, implying the existence of different enzymatic mechanisms for NendoU in coronaviruses and arteriviruses (5).

The results of previous studies have indicated that Nsp15 is important for nidovirus replication. More recent studies have shown that the replacement of the conserved Asp6408 in HCoV-229E Nsp15 with alanine (Ala) completely abolishes its EndoU activity and viral RNA synthesis, thus rendering the virus unrecoverable. A similar result was obtained in an MHV Nsp15 mutant in which Ala was substituted for Asp324 (24, 26). The results reported by Kang et al. indicated that Asp-324 is an important amino acid for the ionic-bond network because the mutant protein is insoluble when MHV Nsp15 was expressed in *Escherichia coli* (26). Taken together, these results suggest that the failure of Nsp15 to fold correctly may play an indirect role in viral replication by affecting the proteolytic processing of the neighboring components by preventing itself from folding correctly, ultimately leading to a nonviable phenotype (32). Furthermore, these findings regarding coronavirus Nsp15 demonstrate its critical function in the evasion of the dsRNA sensors in macrophages and suggest that the disruption of the stability of Nsp15 in coronaviruses may be helpful for designing new live-attenuated vaccines (19).

In a previous study, Nsp15 was found to be active as a hexamer. This finding was confirmed for the Nsp15s in several coronaviruses, including those of MHV, SARS-CoV, HCoV-229E and turkey coronavirus Nsp15 (25, 27, 33, 34). Furthermore, the basic biofunctional unit of SARS-CoV Nsp15 was confirmed to be a hexamer (33). Multiple sequence

alignment and the site-directed mutagenesis experiments using SARS-CoV Nsp15 showed that the N-terminal domain was essential for the oligomerization of Nsp15 and that destruction of this motif strongly affected the catalytic activity of the enzyme (33). A previous study of the oligomerization influence on SARS-CoV Nsp15 activity showed that a mutant lacking the 28 N-terminal residues and 11 C-terminal residues was assumed a monomeric rather than a hexameric form, and the stabilization of the catalytic loop (residues 234 to 249) by the supporting loop (residues 276 to 295) was required to maintain its enzymatic activity. In addition, the supporting loop on the C-terminal domain was supported by the NTD of the adjacent subunit (13). Therefore, the disruption of the hexameric state of Nsp15 can indirectly impact the two reactive histidines, namely, His234 and His249, thus abolishing its enzymatic activity.

In this study, we performed oligomeric and functional analyses of PDCoV Nsp15 to elucidate the mechanism underlying the function of NendoU during nidovirus replication and to identify potential drug targets for controlling PDCoV. Our data indicate that PDCoV Nsp15 exists as a dimer and monomer rather than as a hexamer in solution and suggest that the dimeric form of PDCoV Nsp15 may represent an intermediate in the evolutionary process of nidoviruses. Moreover, our results that PDCoV Nsp15 functions as a dimer provide a basis for better understanding of the conservative structural basis and catalytic mechanism of NendoU.

Results

The predicted three-dimensional structure of PDCoV Nsp15

The predicted three-dimensional structure of PDCoV Nsp15 is a homo-hexamer: two monomers interact with each other and form a hexamer with the NTDs facing towards inside and the C-terminal domains (CTD) outwards. In addition, the hexamer resembles a triangular scaffold to stand still (Fig. 1A); the basic oligomeric unit is a dimer and the N-terminal domain is important for the oligomerization (Fig. 1B and 3B). In addition, the monomer consists of three parts: the intact N-terminal domain (Asn-1 to Arg-167), the C-terminal domain (Pro-193 to Gln-327) and a middle linker domain (LKD; Tyr-168 to Thr-192) (Fig. 1C).

The oligomerization of PDCoV Nsp15 differs from that of other CoVs Nsp15s

The size-exclusion chromatography results of PDCoV Nsp15 show that it is not a hexamer but mainly a monomer and a dimer (Fig. 2A and B). Thus, PDCoV (*Deltacoronavirus*), SARS-CoV (*Betacoronavirus*), and PEDV (*Alphacoronavirus*), as three representative viruses of the *Coronaviridae*, were selected among all coronaviruses for Nsp15 oligomerization analysis among the whole coronaviruses to compare their different oligomeric states *in vitro*. In our work, low production of wild-type protein was also observed due to its bacterial toxicity, which has been previously reported (20, 33). Previous studies have shown that the key catalytic site histidine does not participate in stabilizing functional oligomerization in coronaviruses and arteriviruses (20, 33). According to the sequence alignment results, the catalytic sites of His219, His234 and Lys269 in PDCoV are highly conserved compared with those in SARS-CoV and PEDV Nsp15s. Furthermore, several

substrate binding sites present in PDCoV Nsp15 (Thr273, Asp276, Asp 305, Tyr323) were also conserved at the equivalent sites in SARS-CoV Nsp15 (Ser293, Asp296, Asp323, and Tyr342) (Fig. 3C). According to the conserved catalytic sites, the Nsp15 mutants (PDCoV: H219A, H234A, and K269A; PEDV: H241A; SARS-CoV: H234A) were constructed based on amino acid sequence alignment and high yields of these proteins were harvested (reached approximately 4 to 8 mg/liter).

The size-exclusion chromatography results revealed that the oligomeric forms of PDCoV Nsp15 were a dimer and a monomer (approximately 78.5 kDa and 33.3 kDa, respectively). In contrast, both PEDV Nsp15 and SARS-CoV Nsp15 were hexamers (approximately 228.6 kDa) (Fig. 2A). The peak elution volumes of PDCoV Nsp15 were approximately 15.43 mL and 13.92 mL. PEDV and SARS-CoV Nsp15s showed similar peak elution volumes of approximately 12.07 mL, which were reflected by the bio-standard protein elution results (Fig. 2B). To further verify the specific distributions of these oligomers, we performed an analytical ultracentrifugation experiment. The hexamer proportions of PEDV and SARS-CoV Nsp15s were approximately 81.2% and 91.4%, with predicted molecular weights (MWs) of approximately 187.0 kDa and 218.0 kDa, respectively (Fig. 2D). In the case of PDCoV Nsp15, dimers and monomers occupied approximately 36.1% and 47.5%, with predicted MWs of approximately 81.1 kDa and 37.5 kDa, respectively (Fig. 2E). The calculated MWs and the sedimentation coefficient ($S_{20,W}$) data are shown in Table 1. The proteins used in the size-exclusion chromatography experiment were then visualized by SDS-PAGE (Fig. 2C).

In conclusion, our result verified that

the oligomerization of PDCoV Nsp15 was different from that of other CoV Nsp15s.

The NTD of PDCoV Nsp15 is important for its dimerization

The three-dimensional structure of SARS-CoV Nsp15 (PDB:2rhb) consists of six homomonomers and forms a compact homo-hexamers via the interaction of one NTD (1S-27I) with the other CTD (Fig. 3A). The predicted structure of PDCoV Nsp15 shows that it is also a homo-hexamers and that part of the NTD is involved in its higher oligomerization (Fig. 1A and 3B).

To verify that part of the NTD region (1N-27N) participates in the dimerization of PDCoV Nsp15, we analyzed a PDCoV Nsp15 mutant with its NTD (1N-27N) truncated, called PDCoV Nsp15 (N-terminal truncated), and a PDCoV Nsp15 NTD (1N-27N) mutant replaced with the SARS-CoV Nsp15 NTD (1N-27S), called PDCoV Nsp15 (N-terminal replaced) in gel chromatography experiments. The elution peaks of PDCoV Nsp15 (N-terminal truncated) were approximately 15.73 mL and 14.14 mL, with predicted MWs of approximately 28.0 kDa (monomer) and 69.4 kDa (dimer) (Fig. 4A), respectively, based on the bio-standard protein elution results (Fig. 4B). The main elution volumes of PDCoV Nsp15 (N-terminal replaced) were approximately 15.31 mL and 13.73 mL, with predicted MWs of approximately 35.6 kDa (monomer) and 87.6 kDa (dimer) (Fig. 4A), respectively, which were slightly greater than those of PDCoV Nsp15 (H234A) based on the bio-standard protein elution results (Fig. 2B). The AUC results showed that both dimers and monomers were present in PDCoV Nsp15 (N-terminal truncated), and they represented approximately 19.8% and 61.0% with predicted MWs of approximately 72.9 kDa

and 37.1 kDa, respectively. In addition, few tetramers (approximately 136.0 kDa) were also observed (Fig. 4D). Compared with those in PDCoV Nsp15 (H234A), the percentage of monomers in PDCoV Nsp15 (N-terminal truncated) increased by approximately 13.5%, and the percentage of dimers decreased by approximately 16.3% (Fig. 4D). Additionally, PDCoV Nsp15 (N-terminal replaced) had a high proportion of monomers (approximately 72.9%) with a predicted MW of approximately 36.2 kDa and few other oligomers (Fig. 4E). The calculated MWs and the sedimentation coefficient ($S_{20,W}$) data of the AUC are shown in Table 1. The proteins eluted in the size-exclusion chromatography experiment were then visualized by SDS-PAGE (Fig. 4C).

In addition to the fact that NTD of PDCoV Nsp15 is important for its dimerization, which has been validated in the N-terminal truncated mutant. The reason to explain why PDCoV Nsp15 is a dimer and monomer but not a hexamer remains unclear because the oligomeric form of PDCoV Nsp15 (N-terminal replaced) remains almostly the same as that of PDCoV Nsp15 (H234A) *in vitro*, and it suggests that there should be other regions impeding the hexamerization in PDCoV Nsp15. Thus, the following experiments were performed.

The region (251H-261V) of PDCoV Nsp15 rendering the PDCoV Nsp15 fails to form a hexamer

The structural alignment of SARS-CoV and PDCoV Nsp15 showed that the Asp104 to Ser108, Leu155 to Glu160, and His251 to Val261 regions of PDCoV Nsp15 (Fig. 3C) corresponded to the sequences of the Asp106 to Ala115, Thr166 to Tyr178, and Gln259 to Phe279 regions of SARS-CoV

Nsp15, respectively (Fig. 5A). In addition, all these three loops formed by SARS-CoV Nsp15 are longer than those formed by PDCoV Nsp15, especially the loop formed by the region from Gln259 to Phe279 (Fig. 5A). Two equivalent-region substitution mutants in SARS-CoV Nsp15 were constructed and purified (SARS-CoV Nsp15_{T166-Y178} was not successfully purified). The mutant SARS-CoV Nsp15_{D259-F279} protein was harvested, purified, and used in gel chromatography experiments. The two peak elution volumes of SARS-CoV Nsp15_{D259-F279} were approximately 12.72 mL, corresponding to a tetramer (approximately 152.8 kDa), and approximately 14.15 mL, which was calculated to be a dimer (approximately 68.8 kDa) (Fig. 5B), as reflected by the bio-standard protein elution results (Fig. 5C). In addition, the peak elution volume of SARS-CoV Nsp15 (N-terminal replaced), which was a mutant NTD (1N-27S) of SARS-CoV Nsp15 replaced with NTD (1N-27N) of PDCoV Nsp15, was 11.84 mL with a predicted MW of approximately 259.4 kDa, and it was predicted to be a hexamer (Fig. 5F). The proteins from the size-exclusion chromatography experiment were visualized by SDS-PAGE (Fig. 5D). The AUC experimental results showed that the oligomeric formation completely changed into a mixture of approximately 83.8% monomers (approximately 36.7 kDa), 14.6% dimers (approximately 77.9 kDa), and some higher-order oligomers in solution (Fig. 5E). The calculated protein MWs and sedimentation coefficient ($S_{20,W}$) data are shown in Table 1.

In conclusion, this completely oligomeric change found in SARS-CoV Nsp15_{D259-F279} indicated that the region (251H-261V) of PDCoV Nsp15 could be a reason to explain why PDCoV Nsp15 fails

to form a hexamer. In addition, both of the oligomeric form in SARS-CoV Nsp15 (N-terminal replaced) and PDCoV Nsp15 (N-terminal replaced) remains the same as those of SARS-CoV Nsp15 (H234A) and PDCoV Nsp15 (H234A), which is another evidence to prove that NTD is important for their dimerization but not the hexamerization.

PDCoV Nsp15 is active as a dimer

In arterivirus, the biofunctional unit of the PRRSV NendoU is a dimer. Thus, the unit differs from that of MHV and SARS-CoV NendoUs, both of them function as hexamers (27, 33). The predicted structure of PDCoV Nsp15 contains three conserved catalytic sites (His219, His234, and Lys269) and four binding sites (Thr273, Thr276, Asp305, and Tyr323) that form a pocket for RNA substrate binding (Fig. 6A), which was also reflected by the sequence alignment results (Fig. 3C). Furthermore, the interaction between the two monomers in PDCoV Nsp15 was depicted: the NTD on monomer A interacts with the supporting loop on CTD of monomer B. The interactions between the Asp225, Ser227, Pro228, Val229, Ile230 and Gly232 residues on the “Active Loop” and the Asn265, Ser267, Ser268, Lys269 and Cys272 residues on the “Supporting Loop” are depicted. Furthermore, these extensive interactions between the “Supporting Loop” and the adjacent monomer NTD were also analyzed and determined in LIGPLOT (35). Interactions between the residues Asn258, Cys259, Val260, Ser268, Asn270 and Val271 from the “Supporting Loop” and residues Gys9, Tyr10, Tyr11, Lys12, Asn13, and Cys14 of the adjacent monomer NTD are observed (Fig. 6B). To further verify the enzymatic activity of these sites, FRET experiments were performed, and the results

confirmed that these positions were the functional sites on PDCoV Nsp15. The assay results showed the decreased activity of all PDCoV Nsp15 mutants (H219A, H234A K269A, D276A, and N-terminal truncation). PDCoV Nsp15 mutants (T273A, D305A, and Y323A) could not be obtained due to insolubility. Excision by the PDCoV Nsp15 mutants (H219A, H234A and N-terminal truncated) was reduced 5- to 6-fold compared with that by wild-type PDCoV Nsp15, and K269A retained approximately one-third of the activity of wild-type PDCoV Nsp15. In addition, the D276A mutant showed smaller decrease in catalytic activity compared with other mutants. Our experimental results can be explained based on the positions of the predicted catalytic sites within the predicted three-dimensional structure of PDCoV Nsp15 (Fig. 6A). The H234A mutant shows the greatest activity decrease among all of these mutants because it lies in the center of the enzymatic groove (Fig. 6A). Therefore, compared with the other two catalytic sites, H234 may play an important role in the interaction with the RNA substrate. The complete loss of activity observed in the PDCoV Nsp15 (N-terminal truncated) mutant, which was similar to the loss of activity observed in the H234A mutant, may be due to the dimeric disruption of PDCoV Nsp15, which may affect its normal biological function (Fig. 6B). Among the SARS-CoV Nsp15 mutants, the Nsp15_{D259-F279} mutant displayed the highest enzymatic activity, and its activity decreased by 3/4 compared with that of wild-type PDCoV Nsp15. The second most active mutant was the N-terminal truncated mutant, followed by N-terminal replaced mutant, and then, the H234A mutant (Fig. 6C). The proteins from the enzymatic assay were then visualized by SDS-PAGE (Fig. 6D).

Taken together, the enzymatic assay results further verified that the NTD and His251 to Val261 regions were important for the dimerization of PDCoV Nsp15 and that disruption of its dimerization could decrease its enzymatic activity, which suggests that the biofunctional unit of PDCoV Nsp15 may be a dimer *in vitro*. In addition, the predicted catalytic and binding sites on PDCoV Nsp15 could impact its enzymatic activity to different degrees.

The presumption for the evolution of Nidovirales NendoU

As the counterpart of NendoU, XendoU has been reported to be a monomer (36). According to the three-dimensional structural alignment of XendoU and SARS-CoV Nsp15 (Fig. 7B), a similar structural feature on the CTD was found and reflected by the highly conserved catalytic sites of the “Active Loop”, which have also been found in other NendoUs, such as PRRSV Nsp11 and PDCoV Nsp15 (Fig. 7A). We hypothesize that their active loops are stabilized by the supporting loops in PRRSV nsp11, PDCoV and SARS-CoV Nsp15s. However, XendoU, could be active as a monomer via the undergirding support of residues (Lys113 to Lys125 and Asn133 to Phe144), and the additional upper residues of Gln145 to Cys158 could also provide stability to hold up the “Active Loop” (His162 to His178) (13); these interactions and the predicted “Supporting Loop” on XendoU are depicted (Fig. 7A). In PRRSV nsp11, the “Active Loop” (His129 to His144) and the “Supporting Loop” (Val162 to Thr179) stand out from the center compared with these features in XendoU; thus, the supporting loop alone was not sufficient for its stabilization, and dimerization was required for the “Supporting Loop” to make PRRSV Nsp11

functional. In addition, same condition was found in PDCoV Nsp15 with the interaction between the “Active loop” (His219 to His234) and “Supporting loop” (Gln257 to Thr273) (Fig. 7A). In addition, the “Active loop” (His234 to His249) and “Supporting loop” (Lys276 to Ile295) are also found in SARS-CoV Nsp15. However, PDCoV Nsp15 was an exception for being comprised of dimers and monomers among other Nsp15s (Fig. 2A).

Thus, we hypothesize that PDCoV Nsp15 is an intermediate during the NendoU evolutionary process of the development of high-order oligomerization to better exert its function via structural analysis (Fig. 7C).

Discussion

The newly emerged porcine Deltacoronavirus (PDCoV) belongs to the *Deltacoronavirus* family, whose members can cause similar clinical symptoms to those of PEDV. The highest mortality rate is observed in suckling and weaned pigs with no effective vaccination strategies proposed (4, 6). The large-scale outbreak of PDCoV was first emergent in Ohio and Indiana in 2014, and then, PDCoV immediately spread across the USA, Canada, China and Thailand, causing serious economic losses to the pork industry worldwide (37, 38). In addition, few studies on PDCoV Nsp15 have been reported; thus, to clarify its biofunction, three-dimensional structure or oligomeric distribution could help us to better understand its exact function in coronaviruses.

NendoU is highly conserved for specifically recognizing the U-pyrimidine and producing 3'-5' phosphate products (24). In addition, the conserved biofunction of NendoU relies on the conserved catalytic sites (two histidines and one lysine) (Fig.

6A). The stability of the catalytic center in NendoU is the primary requirement to maintain its natural enzymatic capacity, and any degrees of its structural disruption can directly or indirectly destroy its enzymatic activity. The basic biofunctional unit in SARS-CoV Nsp15 is a hexamer (33), and it comprises a dimer of trimers with the NTDs in the center and the CTDs facing outward, allowing them to possess six active sites to better exert their function in SARS-CoV and MHV Nsp15 (27, 31, 39). In addition, for PRRSV nsp11, the dimer is an active unit, and the disruption of its dimerization can markedly impair its endoribonuclease activity (20). Here, we found that both monomers and dimers were present in PDCoV Nsp15. In addition, decreased enzymatic activity was observed in the PDCoV Nsp15 (N-terminal truncation) mutant (Fig. 6C), which indicates that it functions as a dimer. Furthermore, the SARS-CoV Nsp15_{D259-F279} mutant showed a completely oligomeric change from hexamers to a mixture of monomers and dimers, with the monomer predominating in solution. However, SARS-CoV Nsp15 (N-terminal replaced) still remains as hexamer (Fig. 5F), which needs to be further verified *in vivo* via reverse genetics system. An alternative hypothesis that the residues required for hexamer formation were lost or mutated during the evolutionary process in PDCoV Nsp15 is possible, because the region (H251-V261) is 10 amino acids shorter than the equivalent region (D259-F279) on SARS-CoV Nsp15. In conclusion, the disruption of the oligomerization can impair the normal enzymatic activity of NendoU. In addition, further investigations of Nsp15s need to be performed to verify whether their different oligomeric forms impact their biofunction or the interaction with the RTCs and other

nsp5 *in vivo* by using the reverse genetics or replicon systems. In this study, we attempted to screen the PDCoV Nsp15 crystal under various conditions. Unfortunately, we were unable to obtain the structure.

As the counterpart of NendoU, XendoU is also an endoribonuclease and was purified from *Xenopus laevis* oocyte nuclear extracts (29). A previous study revealed that the oligomeric state of XendoU was monomeric, and the three-dimensional structure of XendoU showed that it adopted a different oligomeric pattern to that of NendoU. The support of residues (K113-K125 and N133-F144) undergirding and the additional upper residues (Q145–C158) could also provide stability to hold up the “Active Loop” (H165–H178) with the predicted “Supporting Loop” adjacent to its “Active Loop” to form into a compact structure, with a globular shape (13). In addition, the highly conserved catalytic sites in XendoU (H162, H178, and K224), are also found in PRRSV Nsp11, PDCoV and SARS-CoV Nsp15s on the three-dimensional structural level (Fig. 7A), serving as an additional evidence of their close relationship at evolutionary aspect. The conservative catalytic residues may provide a novel target for drug design against nidoviruses in the future.

Regarding the origin of NendoU, we hypothesize that nidoviruses may acquire this gene from XendoU in eukaryotic cells and this gene may evolve in the virus to better adapt to the outside environment, a possibility which has already been put forward in previous studies (22, 40). The different oligomeric characteristics of XendoU and NendoU further support this hypothesis. In eukaryotic cells, XendoU exists as a monomer, and in the arterivirus PRRSV Nsp11, it exists mainly as a dimer.

In PDCoV Nsp15, we found it was a mixture of monomers and dimers, and in several *Alpha*-, *Beta*- and *Gammacoronavirus* Nsp15s, the proteins have been identified as hexamers (25, 27, 33, 34). Furthermore, according to the molecular clock analysis, the times to which these four coronaviruses could be traced were approximately 2400 BC, 2800 BC, 3300 BC, 3000 BC, corresponding to *Alphacoronavirus*, *Gammacoronavirus*, *Betacoronavirus*, and *Deltacoronavirus*, respectively (4). PDCoV is the second oldest among the four genera. This result reflects the possible evolutionary course among all coronavirus NendoUs. PDCoV Nsp15 is the intermediate status in the transition process of forming a hexamer from the dimeric form in PRRSV nsp11, and all the NendoUs have the same ancestor, namely, XendoU (Fig. 7C). In addition, a relevant study showed that approximately half of the proteins could interact with other copies of themselves and assemble into homomeric complexes, which was often assumed to be a functionally beneficial result of evolutionary selection (41).

Experimental procedures

The three-dimensional structure prediction

The predicted three-dimensional structure of PDCoV Nsp15 was accomplished in the SWISS-MODEL website (<https://swissmodel.expasy.org/>) and then the structural figures were generated with the PyMOL molecular visualization system (Schrödinger).

Gene cloning and plasmid constructs

The genes encoding Nsp15s were cloned from the PDCoV strain CHN-HN-2014 (GenBank accession number KT336560) and the PEDV FJZZ strain (GenBank accession number

KC140102.1). A codon-optimized SARS-CoV Nsp15 gene (GenBank accession number NP_828872.1; gi:29837507) was synthesized by GenScript Corporation (GenScript, Nanjing, China). The PDCoV Nsp15 mutants (H234A, N-terminal truncated, N-terminal replaced), the SARS-CoV Nsp15 mutants (H234A, N-terminal truncated, and N-terminal replaced) and the PEDV Nsp15 mutant (H241A) used in the analytical ultracentrifugation and size-exclusion chromatography experiments were separately cloned into the pET-42b (+) vector with the *NdeI* and *XhoI* restriction sites and a His6 tag was added at the C-terminal terminus. The alanine-substituted PDCoV Nsp15 mutants (H219A, H234A, K269A, T273A, D276A, D305A, and N-terminal truncated, each with a C-terminal GST tag) were cloned into the pGEX-6p-1 vector by homologous recombination with a C-terminal GST tag for the enzymatic assays. In addition, pET-30a (+) and pET-28a (+) containing the wild-type PDCoV Nsp15 gene with a C-terminal His6 tag were transformed into *Escherichia coli* DE3 to obtain the wild-type PDCoV Nsp15. For the oligomerization experiment, several important sequences of Phe145-Ile164 and His251H-Val261 on PDCoV Nsp15 were replaced by the equivalent sequences of Thr152-Phe179 and Asp259-Phe279 on SARS-CoV Nsp15 to create SARS-CoV nps15_{T152-F179} and SARS-CoV nps15_{D259-F279}, respectively. These constructs, each with a His₆ tag at the C-terminus, were cloned into pET-42b(+) after the digestion of the plasmid with the *NdeI* and *HindIII* restriction enzymes. All of the point mutations and sequence substitution mutations were constructed by the overlapping PCR technique and were

confirmed by the GenScript Company.

Protein expression and purification

The recombinant plasmids described above were transformed into the *E. coli* strain Trans BL21 (DE3) pLysS (Beijing TransGen Biotech, Co., Ltd). The cells transformed with plasmids encoding proteins with GST tags were cultured at 37°C in LB medium containing 50 µg/mL ampicillin. LB medium containing 50 µg/mL kanamycin was used for the cells expressing proteins with His6 tags. When the OD₆₀₀ value of the cell density reached 0.6-0.8, the cells were induced with 0.8 mM IPTG (isopropyl β-D-1-thiogalactopyranoside). To maximize the protein yield, the cells expressing proteins with GST tags were cultured at 37°C for an additional 4 hours. Protein expression and purification were conducted according to our previously reported procedure (19).

The harvested proteins were further purified on a Superdex 200 gel filtration column (GE Healthcare) and were washed with buffer B₂ (20 mM Tris-HCl and 200 mM NaCl, pH 7.4) when the volume of the filtered protein was less than 2.0 mL in the condensing column for centrifugation at 4°C. The proteins were flash-frozen in liquid nitrogen and stored at -80°C until used in biochemical analyses. The concentrations of PDCoV, SARS-CoV and PEDV Nsp15 mutant proteins were determined based on the absorbance values of the samples at 280 nm (A₂₈₀) using a DS-11 FX+ spectrophotometer combined with a highly sensitive 1-µL UV-Vis absorbance spectrophotometer (DeNovix, Inc.).

Size-exclusion chromatography assay

The PDCoV Nsp15 mutants (H234A, N-terminal truncated, and N-terminal

replaced), the SARS-CoV Nsp15 mutants (H234A, N-terminal truncated, N-terminal replaced, and D259D-F279), and the PEDV Nsp15 mutant (H241A) were purified through a Ni-NTA high-affinity filter and then passed through a HiLoad Superdex 200 gel filtration column (GE Healthcare) in elution buffer (20 mM Tris-HCl, 200 mM NaCl pH 7.4) at a flow rate of 0.8 mL/min at 4°C. For the analysis of oligomerization, approximately 1 mg of each protein was subjected to chromatography on a Superdex 200 10/300 GL column in the same elution buffer described above at a flow rate of 0.5 mL/min at 4°C, and the eluted proteins were then assessed by SDS-PAGE analysis. Size-exclusion standards were separated on the column following our previously reported procedure (19). The obtained data were analyzed using Origin 8.0 software. The predicted weight-averaged molar masses were calculated using DNASTAR (version7.1) software.

Analytical ultracentrifugation assay

To confirm the MWs of the individual proteins, sedimentation velocity analysis was conducted in an XL-A model centrifuge (Proteome Lab) at 18°C and 45,000 rpm in 400- μ L double-sector cells. The sedimentation boundary was monitored every 3 min at a wavelength of 280 nm, resulting in 110 scans. The collected data were analyzed using Sedfit software with the model-based distribution of Lamm equation solutions $c(s)$. The data obtained from the size-exclusion chromatography experiments and sedimentation velocity analysis were transformed into curves for analysis in Origin 8.0 software. DNASTAR (version7.1) software was used for protein weight-averaged molar mass prediction.

Enzymatic activity assay

The endoribonuclease activity assay was performed as follows: the wild-type PDCoV Nsp15 and mutant proteins (H219A, H234A, K269A, D276A, and N-terminal truncated) with GST tags at their C-terminal ends and the GST protein as a negative control, each at a concentration of 2 μ M were mixed with 1 μ M RNA substrate (5'-6-FAM-dA-rU-dA-dA-6-TAMRA-3', purchased from GenScript Corporation) (32) in the reaction buffer [50 mM KCl, 50 mM HEPES (pH 7.5), 5 mM MnCl₂ and 1 mM dithiothreitol dissolved in water with 0.1% diethyl-pyrocabonate] and incubated at 25°C for 30 min. The same protocol was used to assess the endoribonuclease activity of the SARS-CoV Nsp15 mutants (H234A, N-terminal truncated, N-terminal replaced, and D259-F279) with the His₆ tag. The CFX96 Touch™ Real-Time PCR Detection System (Bio-Rad Laboratories) was used to quantify the FAM value of each protein for 30 min at wavelengths ranging from 492 nm to 518 nm every 30 seconds. Each protein was assayed three times, and the obtained data were analyzed via GraphPad Prism software 5.0 (GraphPad Software Inc., CA). The values obtained in the triplicate measurements are shown. All of the proteins tested in this assay were also analyzed by SDS-PAGE.

Sequence alignment and phylogenetic tree analysis

The genes encoding SARS-CoV (JF29292), PEDV (KU558702), and PDCoV Nsp15s (KP757891) were separately cloned from the full-length genomes of these three viruses, and the amino acid prediction results were obtained by analyzing the gene sequences using DNASTAR (version7.1) software. The amino acid sequences of SARS-CoV, PEDV and PDCoV Nsp15s were prealigned on the website server of

Clustal Omega (<https://www.ebi.ac.uk/Tools/msa/clustalo/>), and the resulting file was then uploaded to the ESPript 3 website (<http://esprict.ibcp.fr>) to produce the final alignment result. MEGA 6.0 software was used to build the phylogenetic tree to visualize the evolutionary relationships between *Nidovirales* and *Coronaviridae* via the distance-based neighbor-joining method. Bootstrap values were calculated from 1,000 replicates of the alignment. The different subgenotypes are indicated.

Nucleotide sequence accession numbers

The NCBI accession numbers of the sequences referred in this study are listed as follows: PDCoV (porcine Deltacoronavirus, KP757891), SARS-CoV (SARS coronavirus wtic-MB, AGT21317), PEDV (porcine epidemic diarrhea virus, AIM47753), HCoV-229E (human coronavirus 229E, AGT21366), TGEV (transmissible gastroenteritis virus virulent Purdue, ABG89333), MHV (murine hepatitis virus strain A59 NP_740619), IBV (turkey coronavirus, ABW81426.1), PRRSV (porcine respiratory and reproductive syndrome virus strain WUH3, ADO33722), EAV (equine arteritis virus, NP_705592), SHFV (simian hemorrhagic fever virus, AHH54245), LDV (lactate dehydrogenase-elevating virus, AAA74104), and XendoU (*Xenopus laevis*, NP 001081040.1).

Acknowledgements: We thank research associates at the Center for Protein Research (CPR), Hua Zhong Agricultural University, for technical support.

Conflict of interest statement: The authors have declared that no conflict of interest exists.

Author contributions: A. Z. and Y. S. designed the experiment. A. Z., Z. S., G. W., J. S., and Q. X. performed the experiments, A. Z. and Y. S. analyzed the corresponding results. A. Z. wrote the paper with Y. S. and G. P..

FOOTNOTES

Funding was supported by the National Key R&D Plan of China (No. 2018YFD0500100), the National Natural Science Foundation of China (Grant No. 31702249 and 31722056), the China Postdoctoral Science Foundation (grant No.2017M612484) and the Natural Science Foundation of Hubei Province of China (Grant No. 2016CFA069).

References

1. Nga PT, Parquet Mdel C, Lauber C, Parida M, Nabeshima T, Yu F, Thuy NT, Inoue S, Ito T, Okamoto K, Ichinose A, Snijder EJ, Morita K, Gorbalenya AE. (2011) Discovery of the first insect nidovirus, a missing evolutionary link in the emergence of the largest RNA virus genomes. *PLoS pathogens* **7**:e1002215.
2. Vasilakis N, Guzman H, Firth C, Forrester NL, Widen SG, Wood TG, Rossi SL, Ghedin E, Popov V, Blasdel KR, Walker PJ, Tesh RB. (2014) Mesoniviruses are mosquito-specific viruses with extensive geographic distribution and host range. *Virology journal* **11**:97.
3. Cong Y, Verlhac P, Reggiori F. (2017) The Interaction between Nidovirales and Autophagy Components. *Viruses* **9**.
4. Woo PC, Lau SK, Lam CS, Lau CC, Tsang AK, Lau JH, Bai R, Teng JL, Tsang CC, Wang M, Zheng BJ, Chan KH, Yuen KY. (2012) Discovery of seven novel Mammalian and avian coronaviruses in the genus deltacoronavirus supports bat coronaviruses as the gene source of alphacoronavirus and betacoronavirus and avian coronaviruses as the gene source of gammacoronavirus and deltacoronavirus. *Journal of virology* **86**:3995-4008.
5. Nedialkova DD, Ulferts R, van den Born E, Lauber C, Gorbalenya AE, Ziebuhr J, Snijder EJ. (2009) Biochemical characterization of arterivirus nonstructural protein 11 reveals the nidovirus-wide conservation of a replicative endoribonuclease. *Journal of virology* **83**:5671-5682.
6. McCluskey BJ, Haley C, Rovira A, Main R, Zhang Y, Barder S. (2016) Retrospective testing and case series study of porcine delta coronavirus in U.S. swine herds. *Preventive veterinary medicine* **123**:185-191.
7. Cao J, Zhang X. (2012) Comparative in vivo analysis of the Nsp15 endoribonuclease of murine, porcine and severe acute respiratory syndrome coronaviruses. *Virus research* **167**:247-258.
8. Balasuriya UB, Carossino M. (2017) Reproductive effects of arteriviruses: equine arteritis virus and porcine reproductive and respiratory syndrome virus infections. *Current opinion in virology* **27**:57-70.
9. Snijder EJ, Kikkert M, Fang Y. (2013) Arterivirus molecular biology and pathogenesis. *The Journal of general virology* **94**:2141-2163.
10. Guo Z, Chen XX, Li R, Qiao S, Zhang G. (2018) The prevalent status and genetic diversity of porcine reproductive and respiratory syndrome virus in China: a molecular epidemiological perspective. *Virology journal* **15**:2.
11. Balasuriya UB, Carossino M. (2017) Reproductive effects of arteriviruses: equine arteritis virus and porcine reproductive and respiratory syndrome virus infections. *Current opinion in virology* **27**:57-70.
12. Di H, McIntyre AA, Brinton MA. (2018) New insights about the regulation of Nidovirus subgenomic mRNA synthesis. *Virology*.
13. Joseph JS, Saikatendu KS, Subramanian V, Neuman BW, Buchmeier MJ, Stevens RC, Kuhn P. (2007) Crystal structure of a monomeric form of severe acute respiratory syndrome coronavirus endonuclease Nsp15 suggests a role for hexamerization as an allosteric switch. *Journal of virology* **81**:6700-6708.

14. Brierley I, Bournsnel ME, Binns MM, Bilimoria B, Blok VC, Brown TD, Inglis SC. (1987) An efficient ribosomal frame-shifting signal in the polymerase-encoding region of the coronavirus IBV. *The EMBO journal* **6**:3779-3785.
15. Knoops K, Kikkert M, Worm SH, Zevenhoven-Dobbe JC, van der Meer Y, Koster AJ, Mommaas AM, Snijder EJ. (2008) SARS-coronavirus replication is supported by a reticulovesicular network of modified endoplasmic reticulum. *PLoS biology* **6**:e226.
16. Chen Q, Fang L, Wang D, Wang S, Li P, Li M, Luo R, Chen H, Xiao S. (2012) Induction of autophagy enhances porcine reproductive and respiratory syndrome virus replication. *Virus research* **163**:650-655.
17. Gosert R, Kanjanahaluethai A, Egger D, Bienz K, Baker SC. (2002) RNA replication of mouse hepatitis virus takes place at double-membrane vesicles. *Journal of virology* **76**:3697-3708.
18. Bhardwaj K, Sun J, Holzenburg A, Guarino LA, Kao CC. (2006) RNA recognition and cleavage by the SARS coronavirus endoribonuclease. *Journal of molecular biology* **361**:243-256.
19. Deng X, Hackbart M, Mettelman RC, O'Brien A, Mielech AM, Yi G, Kao CC, Baker SC. (2017) Coronavirus nonstructural protein 15 mediates evasion of dsRNA sensors and limits apoptosis in macrophages. *Proceedings of the National Academy of Sciences of the United States of America* **114**:E4251-e4260.
20. Shi Y, Li Y, Lei Y, Ye G, Shen Z, Sun L, Luo R, Wang D, Fu ZF, Xiao S, Peng G. (2016) A Dimerization-Dependent Mechanism Drives the Endoribonuclease Function of Porcine Reproductive and Respiratory Syndrome Virus nsp11. *Journal of virology* **90**:4579-4592.
21. Shi X, Wang L, Li X, Zhang G, Guo J, Zhao D, Chai S, Deng R. (2011) Endoribonuclease activities of porcine reproductive and respiratory syndrome virus nsp11 was essential for nsp11 to inhibit IFN-beta induction. *Molecular immunology* **48**:1568-1572.
22. Posthuma CC, Nedialkova DD, Zevenhoven-Dobbe JC, Blokhuis JH, Gorbalenya AE, Snijder EJ. (2006) Site-directed mutagenesis of the Nidovirus replicative endoribonuclease NendoU exerts pleiotropic effects on the arterivirus life cycle. *Journal of virology* **80**:1653-1661.
23. Bhardwaj K, Guarino L, Kao CC. (2004) The severe acute respiratory syndrome coronavirus Nsp15 protein is an endoribonuclease that prefers manganese as a cofactor. *Journal of virology* **78**:12218-12224.
24. Ivanov KA, Hertzog T, Rozanov M, Bayer S, Thiel V, Gorbalenya AE, Ziebuhr J. (2004) Major genetic marker of nidoviruses encodes a replicative endoribonuclease. *Proceedings of the National Academy of Sciences of the United States of America* **101**:12694-12699.
25. Cao J, Wu CC, Lin TL. (2008) Turkey coronavirus non-structure protein Nsp15--an endoribonuclease. *Intervirology* **51**:342-351.
26. Kang H, Bhardwaj K, Li Y, Palaninathan S, Sacchettini J, Guarino L, Leibowitz JL, Kao CC. (2007) Biochemical and genetic analyses of murine hepatitis virus Nsp15 endoribonuclease. *Journal of virology* **81**:13587-13597.
27. Xu X, Zhai Y, Sun F, Lou Z, Su D, Xu Y, Zhang R, Joachimiak A, Zhang XC,

- Bartlam M, Rao Z. (2006) New antiviral target revealed by the hexameric structure of mouse hepatitis virus nonstructural protein Nsp15. *Journal of virology* **80**:7909-7917.
28. Lauber C, Ziebuhr J, Junglen S, Drosten C, Zirkel F, Nga PT, Morita K, Snijder EJ, Gorbalenya AE. (2012) Mesoniviridae: a proposed new family in the order Nidovirales formed by a single species of mosquito-borne viruses. *Archives of virology* **157**:1623-1628.
29. Laneve P, Altieri F, Fiori ME, Scaloni A, Bozzoni I, Caffarelli E. (2003) Purification, cloning, and characterization of XendoU, a novel endoribonuclease involved in processing of intron-encoded small nucleolar RNAs in *Xenopus laevis*. *The Journal of biological chemistry* **278**:13026-13032.
30. Gioia U, Laneve P, Dlakic M, Arceci M, Bozzoni I, Caffarelli E. (2005) Functional characterization of XendoU, the endoribonuclease involved in small nucleolar RNA biosynthesis. *The Journal of biological chemistry* **280**:18996-19002.
31. Ricagno S, Egloff MP, Ulferts R, Coutard B, Nurizzo D, Campanacci V, Cambillau C, Ziebuhr J, Canard B. (2006) Crystal structure and mechanistic determinants of SARS coronavirus nonstructural protein 15 define an endoribonuclease family. *Proceedings of the National Academy of Sciences of the United States of America* **103**:11892-11897.
32. Ziebuhr J, Snijder EJ, Gorbalenya AE. (2000) Virus-encoded proteinases and proteolytic processing in the Nidovirales. *The Journal of general virology* **81**:853-879.
33. Guarino LA, Bhardwaj K, Dong W, Sun J, Holzenburg A, Kao C. (2005) Mutational analysis of the SARS virus Nsp15 endoribonuclease: identification of residues affecting hexamer formation. *Journal of molecular biology* **353**:1106-1117.
34. Huo T, Liu X. (2015) Crystallization and preliminary X-ray crystallographic analysis of a nonstructural protein 15 mutant from Human coronavirus 229E. *Acta crystallographica. Section F, Structural biology communications* **71**:1156-1160.
35. Laskowski RA, Swindells MB. (2011) LigPlot+: multiple ligand-protein interaction diagrams for drug discovery. *Journal of chemical information and modeling* **51**:2778-2786.
36. Renzi F, Caffarelli E, Laneve P, Bozzoni I, Brunori M, Vallone B. (2006) The structure of the endoribonuclease XendoU: From small nucleolar RNA processing to severe acute respiratory syndrome coronavirus replication. *Proceedings of the National Academy of Sciences of the United States of America* **103**:12365-12370.
37. Ma Y, Zhang Y, Liang X, Lou F, Oglesbee M, Krakowka S, Li J. (2015) Origin, evolution, and virulence of porcine deltacoronaviruses in the United States. *mBio* **6**:e00064.
38. Lorsirigool A, Saeng-Chuto K, Temeeyasen G, Madapong A, Tripipat T, Wegner M, Tuntituvanont A, Intrakamhaeng M, Nilubol D. (2016) The first detection and full-length genome sequence of porcine deltacoronavirus isolated in Lao PDR. *Journal of virology* **161**:2909-2911.
39. Deng X, Baker SC. (2018) An "Old" protein with a new story: Coronavirus endoribonuclease is important for evading host antiviral defenses. *Virology* **517**:157-163.

40. Orr HA. (2009) Fitness and its role in evolutionary genetics. *Nature reviews. Genetics* **10**:531-539.
41. Bergendahl LT, Marsh JA. (2017) Functional determinants of protein assembly into homomeric complexes. **7**:4932.

TABLE 1. Parameters of Sedimentation velocity analysis

| Construct | Predicted MW(kDa) | | | | AUC | | |
|--|-------------------|-------|---------|---------|---------------|---------|---------------|
| | Monomer | Dimer | Hexamer | f/f_0 | $S_{20,w}(S)$ | MW(kDa) | Percentage(%) |
| SARS-CoV Nsp15 (H234A) | 39.2 | - | 234 | 1.51 | 8.639 | 218.0 | 91.4 |
| PEDV Nsp15 (H241A) | 38.1 | - | 228 | 1.48 | 8.212 | 187.0 | 81.2 |
| PDCoV Nsp15 (H234A) | 38.2 | 76.4 | - | 1.40 | 2.88 | 37.5 | 47.5 |
| | | | | | 4.824 | 81.1 | 36.1 |
| PDCoV Nsp15 (N-terminal truncated) | 35.1 | 71.4 | - | 1.40 | 2.672 | 37.1 | 60.9 |
| | | | | | 4.197 | 72.9 | 19.6 |
| PDCoV Nsp15 (N-terminal replaced) | 37.1 | - | - | 1.57 | 2.518 | 36.2 | 72.9 |
| SARS-CoV Nps15 _{D259-F279} | 38.2 | 76.4 | - | 1.29 | 3.099 | 36.7 | 83.8 |
| | | | | | 5.117 | 77.8 | 14.6 |

Figure and figure legends

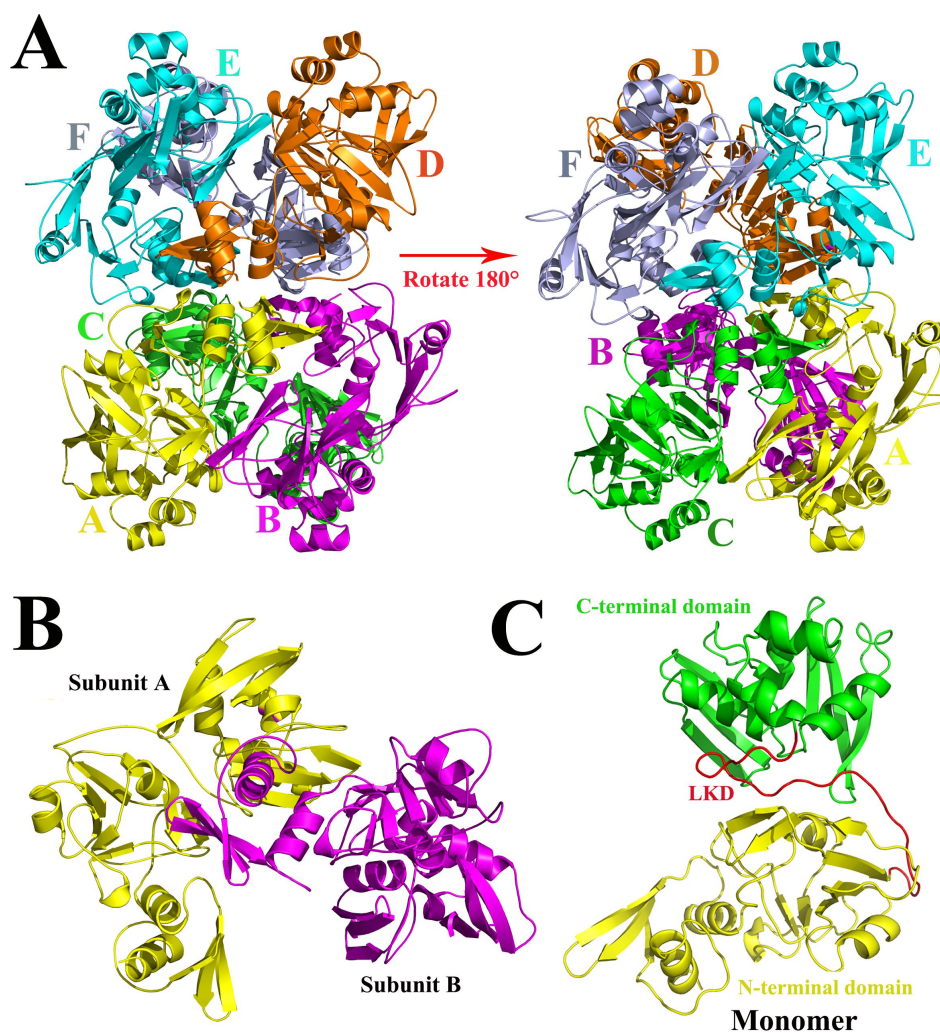


Figure 1. The predicted three-dimensional structure of PDCoV Nsp15. (A) From the side face, the predicted three-dimensional structure of PDCoV Nsp15 was built in the swiss-model website. It consists of six monomers which are depicted and marked in PyMOL software with different colors of yellow, magenta, green, orange, cyan and lightblue for monomer A, B, C, D, E and F, respectively. (B) Two monomers interact with each other closely forming into a dimer with subunit A and subunit B. (C) The monomer of PDCoV Nsp15 consists of three parts: the N-terminal domain (Asn1 to Arg167) in yellow color, the C-terminal domain (CTD; Pro193 to Gln327) in green color and a middle linker domain (LKD; Tyr168 to Thr192) in red color.

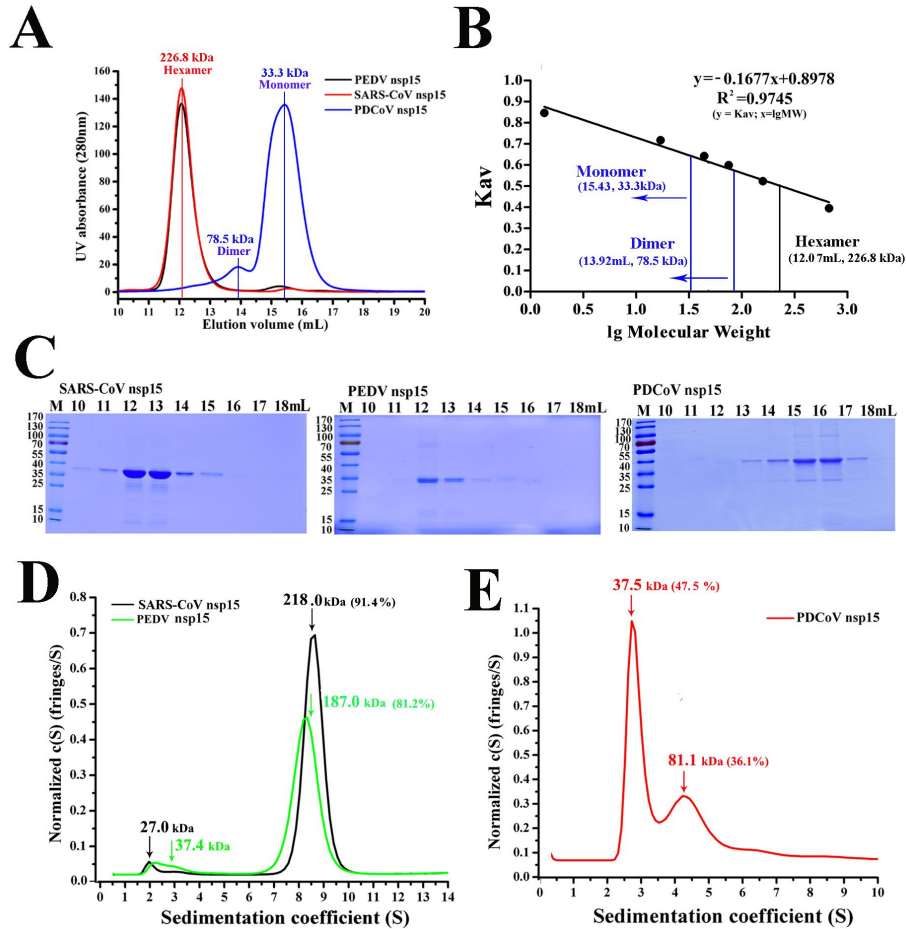


Figure 2. The oligomerization of PDCoV nps15 is different from other CoV nps15s. (A) Size-exclusion experiment of PDCoV Nsp15 (blue), SARS-CoV Nsp15 (red) and PEDV Nsp15 (black). The calculated molecular masses were determined by fitting to the calibration curve as described in panel B. (B) Calculated molecular masses of these Nsp15s peaks with the values obtained for known calibration standards (Bio-Rad and GE Healthcare). The calculated molecular weight of Nsp15 peaks was determined by fitting to the calibration curve ($K_{av} = \text{volumes of elution} [V_{es}/24]$); volumes of elution of 12.07 mL (approximately 226.8 kDa) in SARS-CoV and PEDV Nsp15s (black vertical line), 13.92 mL (approximately 78.5 kDa) and 15.43 mL (approximately 33.3 kDa) in PDCoV Nsp15 (blue vertical line) are depicted. (C) SDS-PAGE analysis of SARS-CoV Nsp15, PEDV Nsp15, and PDCoV Nsp15. The elution volume is labeled as described in panel A. Molecular mass markers are shown. (D and E) Sedimentation velocity analysis of SARS-CoV Nsp15 (black), PEDV Nsp15 (green), and PDCoV Nsp15 (red) with their major peaks of hexamers (approximately 218.0 kDa and 187.0 kDa), dimer (approximately 81.1 kDa) and monomer (approximately 37.5 kDa), respectively. The sedimentation coefficient ($S_{20,W}$) and the calculated molecular weights (MW) are shown in Table 1.

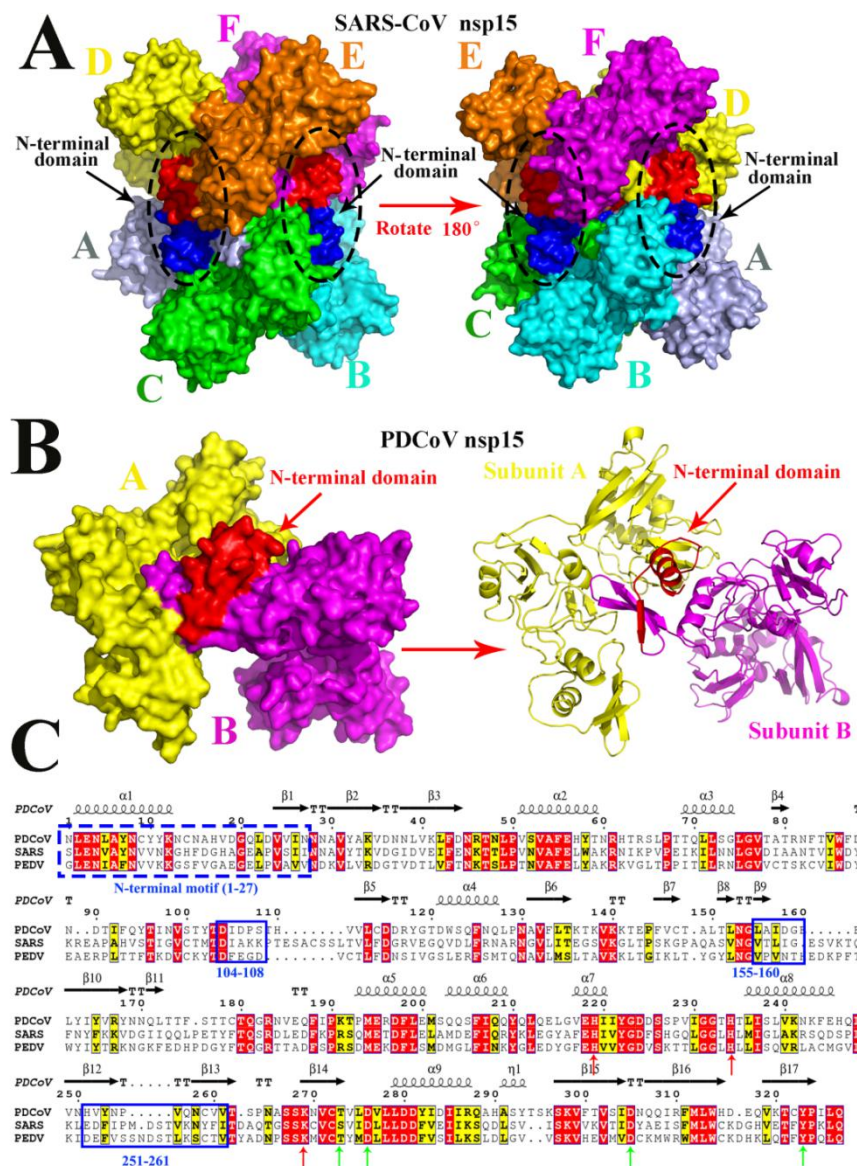


Figure 3. Predicted residues involved in the dimerization of PDCoV nsp15 determined through sequence and structure alignment. (A) The structure of SARS-CoV nsp15 (2rhb) is a homohexamer with six monomers A (lightblue), B (cyan), C (green), D (yellow), E (orange), F (magenta) and three NTDs are shown in red color and the other three NTDs are shown in blue color and are indicated by black arrows. (B) The predicted three-dimensional structure of PDCoV nsp15 which was built in the swiss-model website. Monomer A (yellow) and monomer B (magenta) form a dimer via the interaction with N-terminal domain (red), and the right panel is the cartoon formation of PDCoV nsp15 depicted in PyMOL, Monomer A (yellow) and monomer B (magenta) are interacted with each other through the NTD (red) which are indicated by red arrows. (C) The amino acid sequence alignment of PDCoV, SARS-CoV, and PDCoV Nsp15s. The formal 27 amino acids of these two Nsp15s are depicted with blue dotted line; Asp104 to Ser108, Leu155 to Glu160, and His251 to Val261 residues on PDCoV Nsp15 are depicted with the blue full lines. The conservative sites of three catalytic sites and four binding sites are indicated with red and green arrows, respectively.

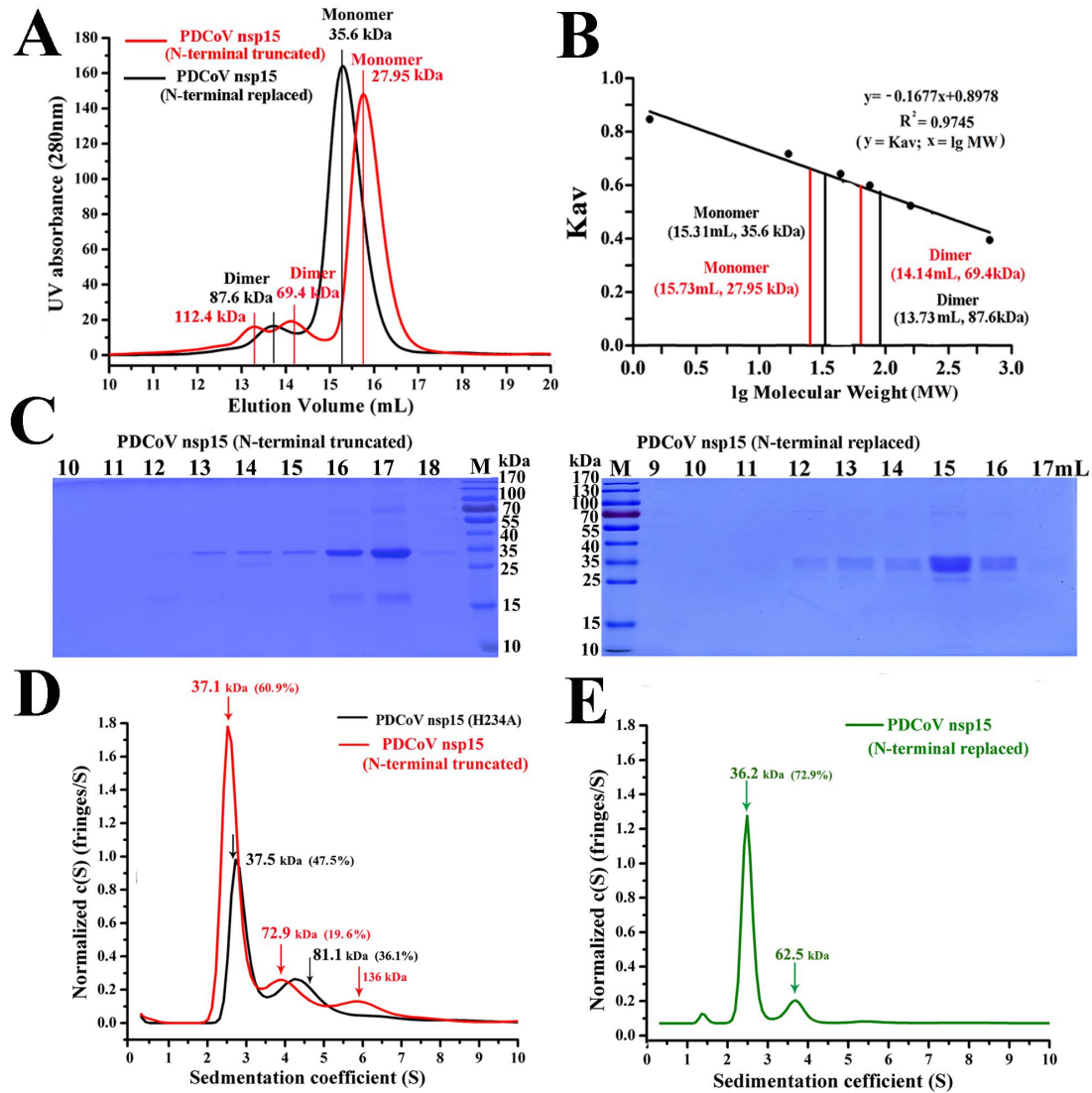


Figure 4. The NTD of PDCoV Nsp15 is important for its dimerization. (A) Size-exclusion experiment with PDCoV nps15 (N-terminal truncated) (red) and PDCoV nps15 (N-terminal replaced) (black). The calculated molecular masses are indicated in red vertical line for N-terminal truncated mutant with three peak volumes corresponding to predicted MWs of approximately 112.4 kDa, 69.4 kDa and 27.9 kDa; and the predicted MWs of N-terminal replaced mutant were approximately 87.6 kDa and 35.6 kDa, they were determined by fitting to the calibration curve as described for panel B. (B) Calculated molecular weights of the Nsp15 protein peaks with the values obtained for known calibration standards (Bio-Rad and GE Healthcare). The calculated molecular weight of Nsp15 peaks was determined by fitting to the calibration curve (K_{av} = volumes of elution [$V_{es}/24$]); (C) SDS-PAGE analysis of PDCoV nps15 (N-terminal truncated) and PDCoV nps15 (N-terminal replaced). The elution volume is labeled as described for panel A. Molecular mass markers are shown. (D and E) Sedimentation velocity analysis of PDCoV nps15 (N-terminal truncated) (red), PDCoV nps15 (H234A) (black) and PDCoV nps15 (N-terminal replaced) (green) with their major peaks is depicted in panel D and F. The sedimentation coefficient ($S_{20,W}$) and the calculated molecular weights (MW) are shown in Table 1.

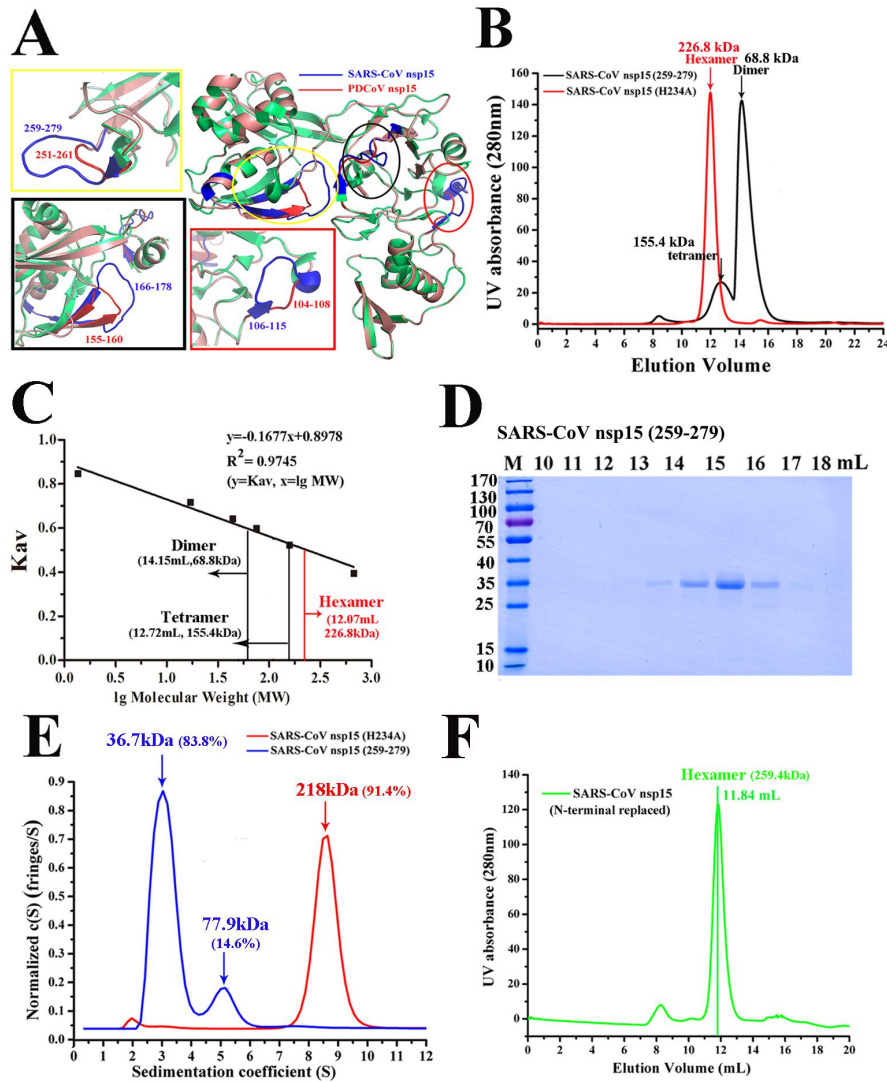


Figure 5. The region (His251-Val261) of PDCoV Nsp15 rendering the PDCoV Nsp15 fails to form a hexamer. (A) The three-dimensional structural alignment of SARS-CoV Nsp15 (PDB 2H85) (green) and PDCoV Nsp15 (salmon). The predicted residues participating in dimerization are depicted with three ellipses and they are drawn in rectangles, the residues of Asp104 to Ser108, Leu155 to Glu160 and His251 to Val261 regions of PDCoV Nsp15 are highlighted in red color and located in red, black, and yellow rectangles, respectively. The corresponding residues of Asp106 to Ala115, Thr166 to Tyr178, and Gln259 to Phe279 regions on SARS-CoV Nsp15 are depicted in blue color. (B) Size-exclusion experiment with SARS-CoV Nsp15_{D259-F279} and SARS-CoV nsp15 (H234A). The calculated molecular masses were determined by fitting to the calibration curve as described in panel C. (C) Calculated molecular weights of Nsp15 protein peaks with the values obtained for known calibration standards (Bio-Rad and GE Healthcare). The calculated molecular weight of Nsp15 peaks was determined by fitting to the calibration curve ($K_{av} = \text{volumes of elution} [V_{es}/24]$) and the two peak volumes of SARS-CoV Nsp15_{D259-F279} were approximately 12.72 mL and 14.15 mL indicated in black vertical lines with the predicted MWs of approximately 155.4 kDa and 68.8 kDa, respectively, in panel B. (D) SDS-PAGE analysis of SARS-CoV Nsp15_{D259-F279}. (E) Sedimentation velocity analysis of SARS-CoV Nsp15_{D259-F279} (blue) and SARS-CoV Nsp15

(H234A) (red) with their major peaks in panel E. The sedimentation coefficient ($S_{20,W}$) and the calculated molecular weights (MW) are shown in Table 1. (F) Size-exclusion experiment result of SARS-CoV nps15 (N-terminal replaced) (green) with the elution volume of approximately 11.84mL and the calculated molecular mass of approximately 259.4 kDa were determined by fitting to the calibration curve as described in panel C.

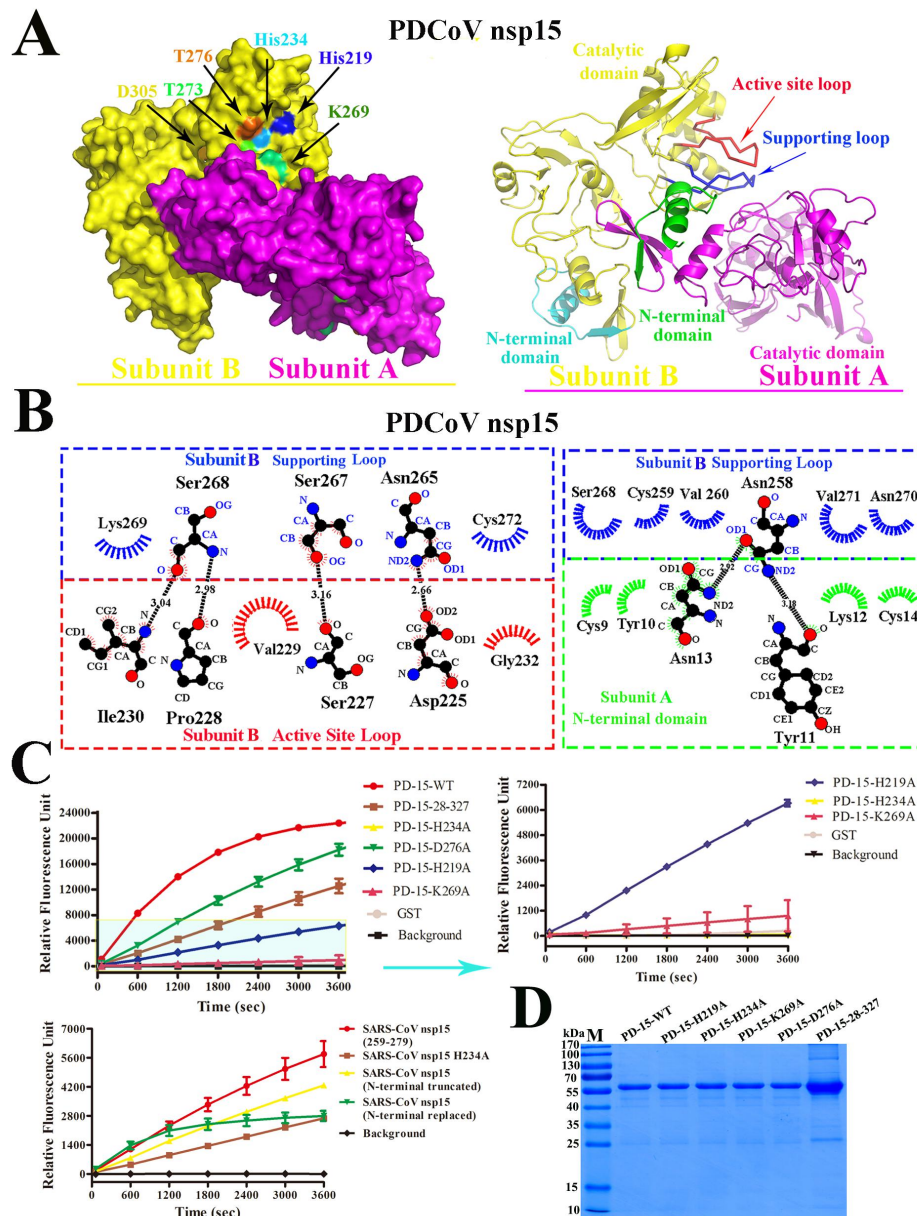


Figure 6. The NendoU activity of PDCoV nps15 and SARS-CoV Nsp15. (A) The predicted structure of dimeric PDCoV Nsp15. The subunit A (magenta) and subunit B (yellow) are tightly interacted with each other, the catalytic sites of His234, His219, Lys269 and binding sites of Thr273, Asp276, and Asp305 are marked with arrows with the color of cyan, blue, green, light green, orange, and yellow, respectively. The right one is the cartoon picture of dimeric PDCoV Nsp15 with subunit A (magenta) and B (yellow) interaction via the interplay of NTD (green) on subunit A and the “Supporting loop” (Asn257 to Cys273) in blue color to stabilize the “Active site loop” (His219 to His234) in red color on subunit B. The NTD of subunit B is in cyan color. (B) Detailed molecular interactions of the “Supporting loop” (blue)

and the “Active site loop” (red) on subunit B with the NTD (green) on subunit A were determined using LIGPLOT. Carbon, oxygen, and nitrogen atoms are shown as black, red, and blue circles, respectively. Hydrogen bonds are shown with black dashed lines between the donor and acceptor atoms with the bond distance. Hydrophobic interactions are shown by arcs with spokes in blue color for the “Supporting loop”, red color for the “Active site loop” on subunit A and green color for the NTD on subunit B which are radiating toward the atoms they interact. (C) FRET-based enzyme activity experiment. The enzymatic activity of the wild-type PDCoV Nsp15 and mutants (H219A, H234A, K269A, D276A and N-terminal truncated) is depicted with different colors. The values of the triplicate experiment results are shown. The enzymatic activity of SARS-CoV Nsp15 mutants (H234A, N-terminal truncated, N-terminal replaced and D259-F279) is depicted. The values of the triplicate experiment results are shown. (D) SDS-PAGE analysis of PDCoV nps15 mutants.

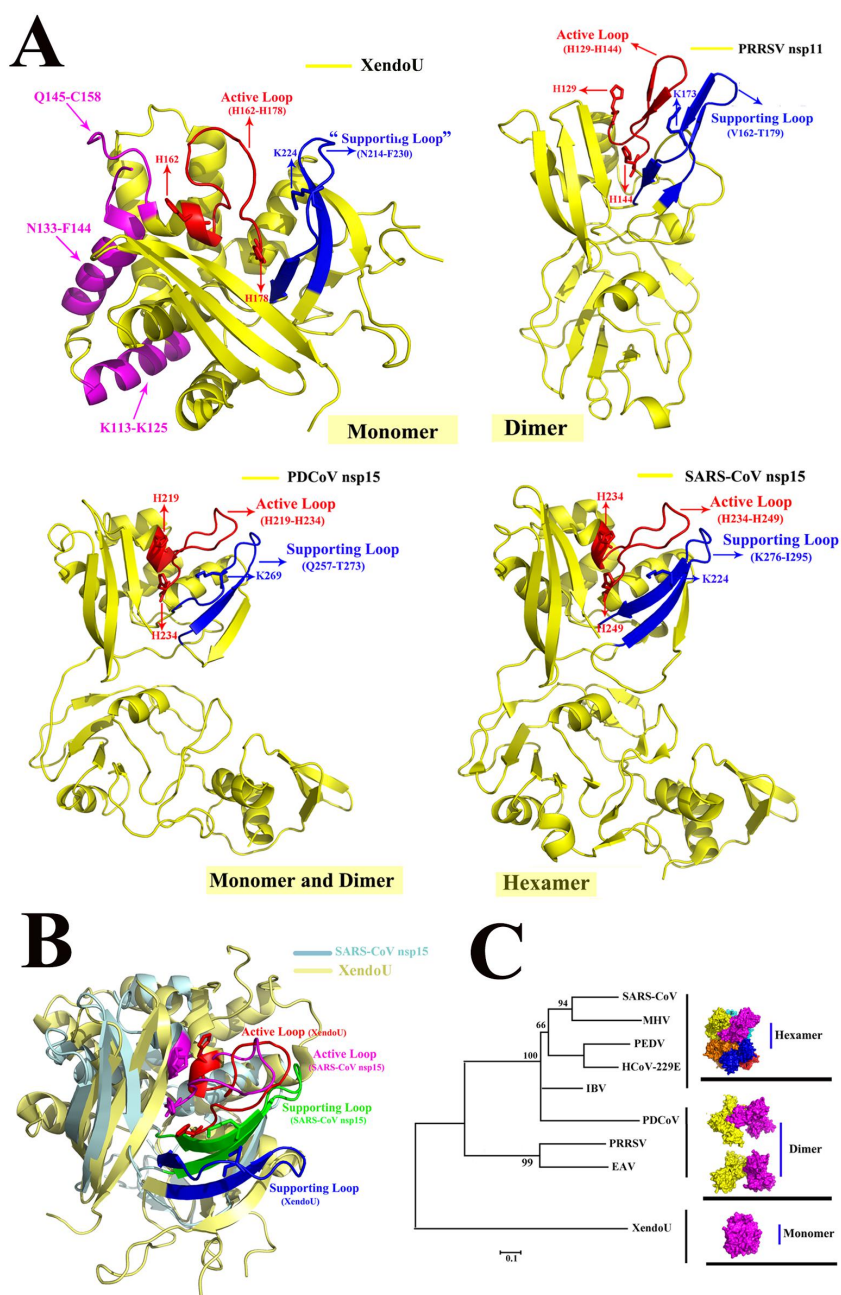


Figure 7. The possible model of the evolutionary process for the nidorivirus XendoU. (A) The monomeric forms of the three-dimensional structures of XendoU (PDB 2C1W), PRRSV nsp11 (PDB: 5DA1), PDCoV Nsp15 (predicted structure) and SARS-CoV Nsp15 (PDB: 2H85) were depicted in yellow color and the catalytic sites of XendoU (His162, His178 and Lys224), PRRSV nsp11 (His129, His144 and Lys173), PDCoV Nsp15 (His219, His234 and Lys269) and SARS-CoV Nsp15 (His234, His249 and Lys289) are indicated with red arrows. The common “Active Loop” and “Supporting Loop” on XendoU (His162 to His178 and Asn214 to Phe230), PRRSV nsp11 (His129 to His144 and Val162 to Thr179), PDCoV Nsp15 (His219 to His234 and Gln257 to Thr273) and SARS-CoV Nsp15 (H234 to H249 and K276 to I295) are indicated with red and blue colors, respectively. Moreover, residues of K113 to K125, N133 to F144 and Q145 to C158 on XendoU are shown in magenta color. (B) The three-dimensional structural alignment of SARS-CoV Nsp15 (light blue) and XendoU (light yellow) are depicted. “Active Loop” and “Supporting Loop” of SARS-CoV Nsp15 are shown in magenta and green colors, respectively. “Active Loop” and “Supporting Loop” of XendoU are shown in red and blue colors, respectively. (C) XendoU is a monomer with magenta color. The dimeric nsp11 is in yellow and magenta colors, and the hexameric *Alpha*-, *Beta*- and *Gamma*-coronavirus Nsp15s comprise six monomers are drawn in different colors. PDCoV Nsp15 is an intermediate and depicted as a dimer in yellow and magenta colors. The phylogenetic tree was analyzed using the distance-based neighbor-joining method in the MEGA package. The different subgenotypes are indicated.

Insight into the evolution of nidovirus endoribonuclease based on the finding that Nsp15 from porcine deltacoronavirus functions as a dimer
Anjun zheng, Yuejun Shi, Zhou Shen, Gang Wang, Jiale Shi, Qiqi Xiong, Liurong Fang, Shaobo Xiao, Zhen F. Fu and Guiqing Peng

J. Biol. Chem. published online June 10, 2018

Access the most updated version of this article at doi: [10.1074/jbc.RA118.003756](https://doi.org/10.1074/jbc.RA118.003756)

Alerts:

- [When this article is cited](#)
- [When a correction for this article is posted](#)

[Click here](#) to choose from all of JBC's e-mail alerts